Forms of Minerals in Biology

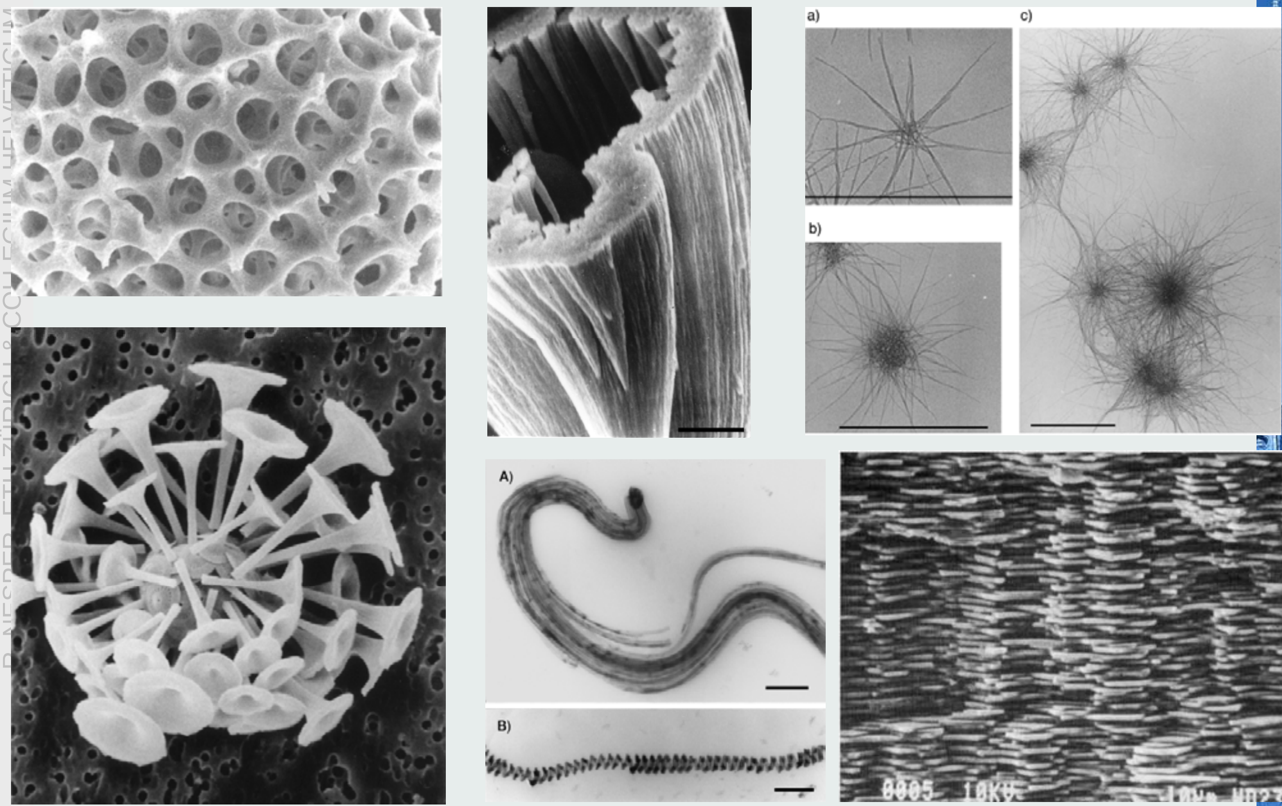

Function of Minerals in Biology

- protection
- motion
- cutting and grinding
- buoyancy
- optical, magnetic and gravity sensing
- storage.

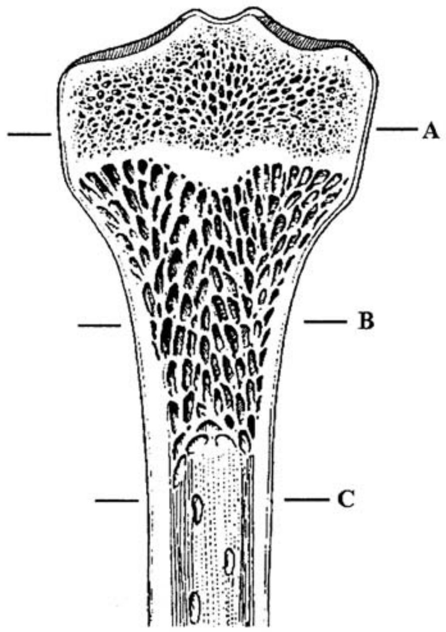

Fig. 2.9 Internal structure of long bone with three different microstructures (A, B and C).

Minerals in Biology

TABLE 11.8 Most Important Biominerals

Chemical Composition	Mineral Phase	Function and Examples
Calcium carbonate $CaCO_3$	Calcite Aragonite Vaterite Amorphous	Exoskeletons (e.g., egg shells, corals, mollusks, sponge spicules)
Calcium phosphates		
$Ca_{10}(OH)_2(PO_4)_6$	Hydroxyapatite (HAP)	Endoskeletons (bones and teeth)
$Ca_{10-x}(HPO_4)_x(PO_4)_{6-x}(OH)_{2-x}$	Defect apatites	
$Ca_{10}F_2(PO_4)_6$	Fluoroapatite	
$Ca_2(HPO_4)_2 \cdot 2H_2O$	Dicalcium phosphate dihydrate (DCPD)	
$Ca_2(HPO_4)_2$	Dicalcium phosphate (DCPA)	
$Ca_8(HPO_4)_2(PO_4)_4 \cdot H_2O$	Octacalcium phosphate (OCP)	
$Ca_3(PO_4)_2$	β-Tricalcium phosphate (TCP)	
Calcium oxalate $CaC_2O_4 \cdot (1 \text{ or } 2)H_2O$	Whewellite Wheddelite	Calcium storage and passive deposits in plants calculi of excretory tracts
Metal sulfates		
$CaSO_4 \cdot 2H_2O$	Gypsum	Gravity sensors
$SrSO_4$	Celestite	Exoskeletons (acantharia)
$BaSO_4$	Baryte	Gravity sensors
Amorphous silica $SiO_n(OH)_{4-2n}$	Amorphous (opal)	Defense in plants, diatom valves, sponge spicules, and radiolarian tests
Iron oxides		
Fe_3O_4	Magnetite	Chiton teeth, magnetic sensors
α,γ-Fe(O)OH	Goethite, lepidocrocite	Chiton teeth
$5Fe_2O_3 \cdot 9H_2O$	Ferrihydrite	Chiton teeth, iron storage

Forms of Minerals in Biology

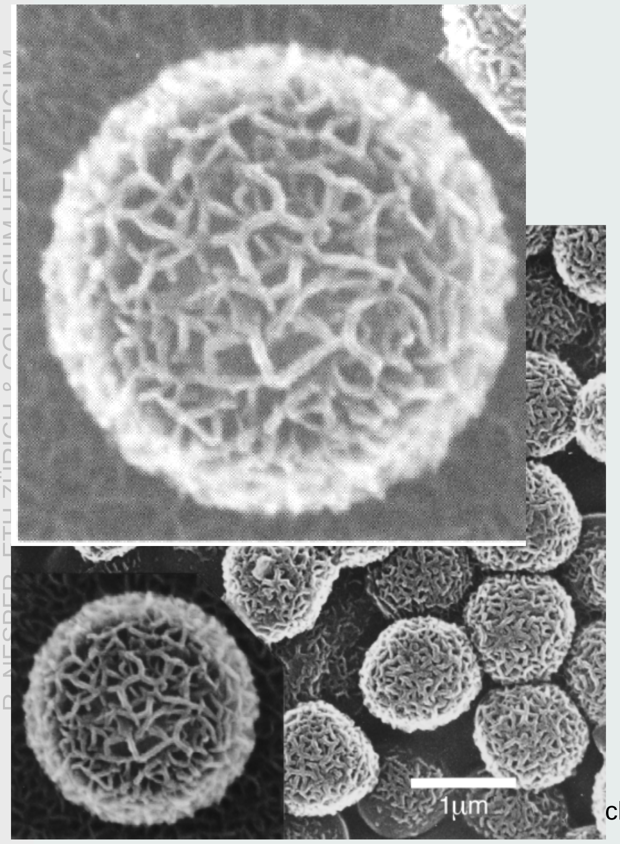

che

Reproducability of Minerals in Biology

Table 2.3 Chemical composition of calcium phosphate (hydroxyapatite) in human and shark enamel

Composition (wt%)	Human enamel	Shark enamel
Ca^{2+}	37.55	37.26
Na^{+}	0.75	0.76
Mg^{2+}	0.27	0.32
PO_4^{3-}	17.68	17.91
CO_3^{2-}	3.6	1.1
F^{-}	0.02	3.65

Silica - deep sea sponge

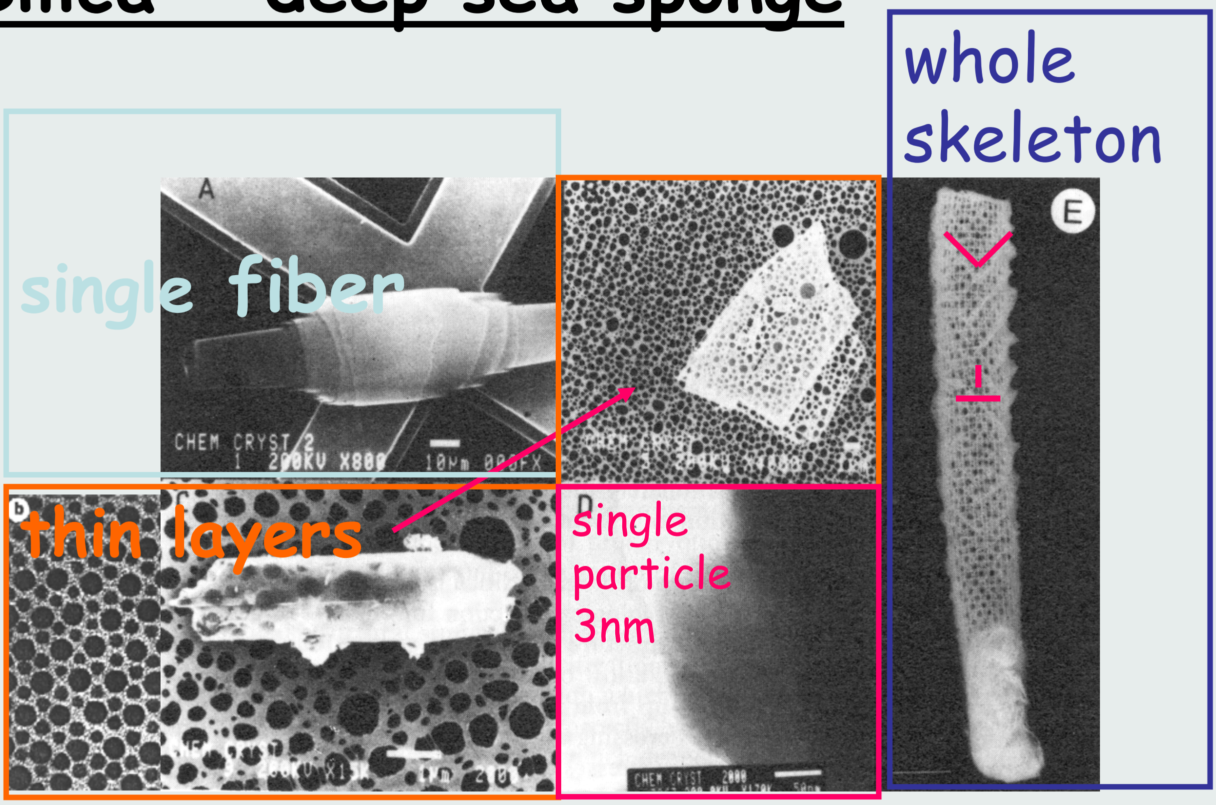

C.C.Perry in S. Mann, J.Webb, R.J.P.Williams, Biomineralization, VCH 1989

Selfassembly

Spontaneous ordering of bimodal ensembles of nanoscopic gold clusters

C. J. Kiely*, J. Fink*†, M. Brust†, D. Bethell† & D. J. Schiffrin†

* *Materials Science and Engineering, Department of Engineering, The University of Liverpool, Liverpool L69 3BX, UK*
† *Department of Chemistry, The University of Liverpool, Liverpool L69 7ZD, UK*

Nature (1998) 396, 444

primary structure

after aging

phase separation

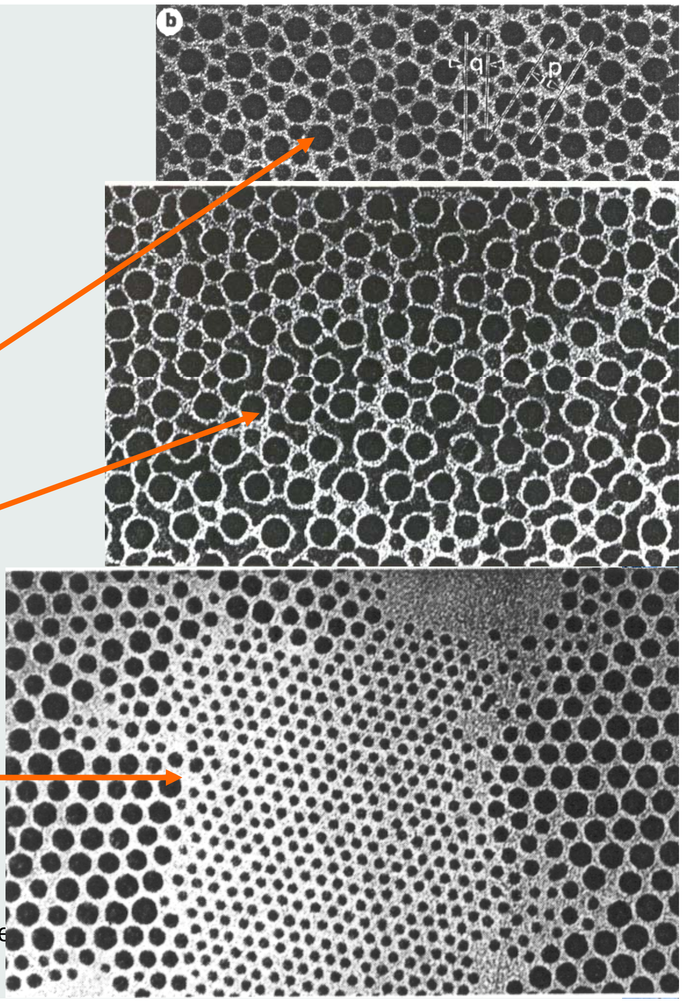

design - two cluster sizes

Advanced Selfassembly

Magnetosomes in algae

S. Mann, R.B. Frankel
in S. Mann, J.Webb,
R.J.P.Williams, Biomineralization,
VCH 1989

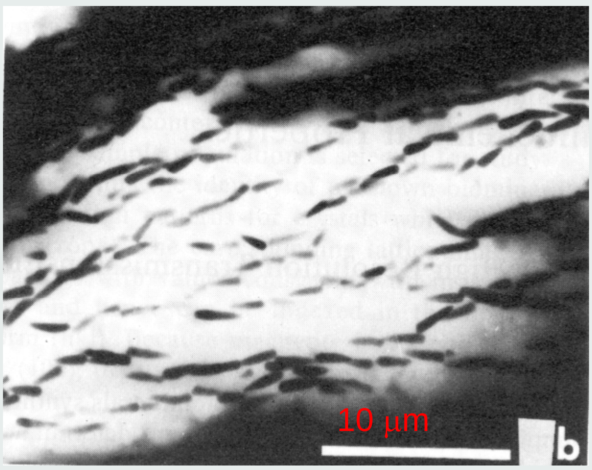

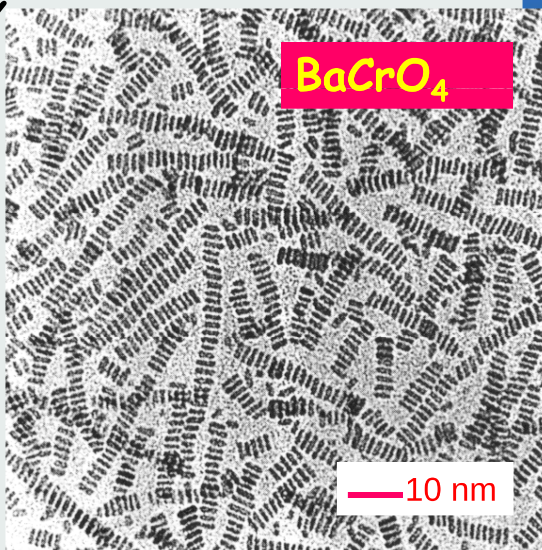

Coupled synthesis and self-assembly of nanoparticles to give structures with controlled organization

Mei Li*, Heimo Schnablegger† & Stephen Mann*

Nature (1999) 402, 393

Bio"mineralization"

Design + Selforganisation

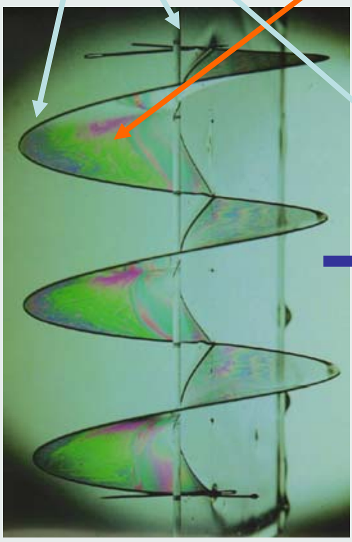

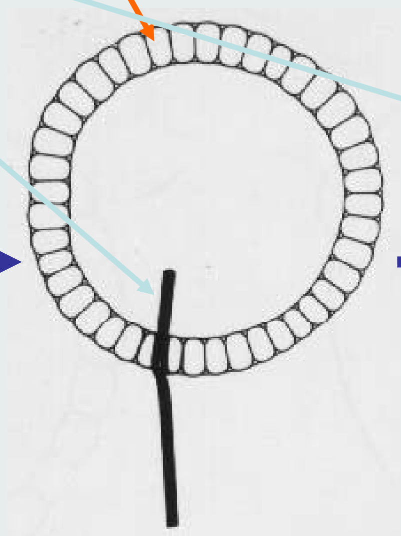

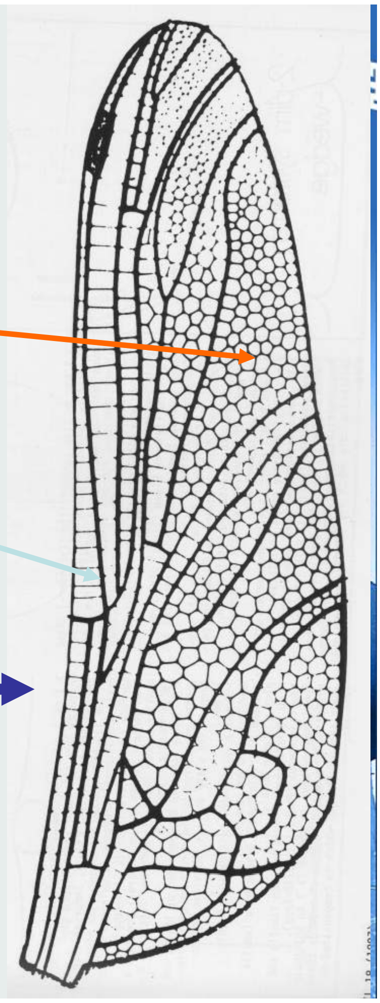

More Complex Forms of Minerals in Biology

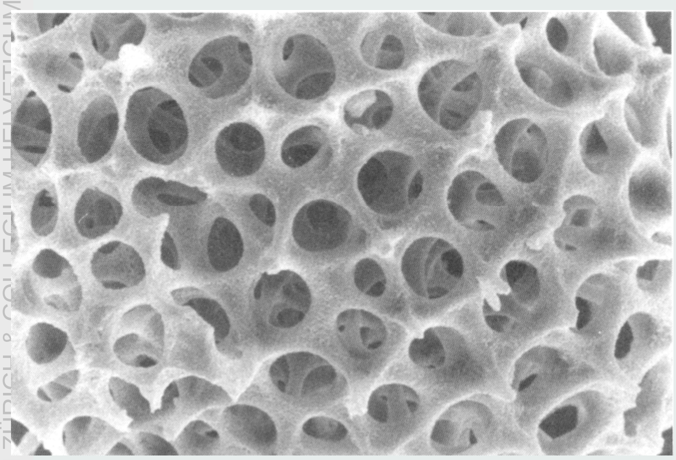

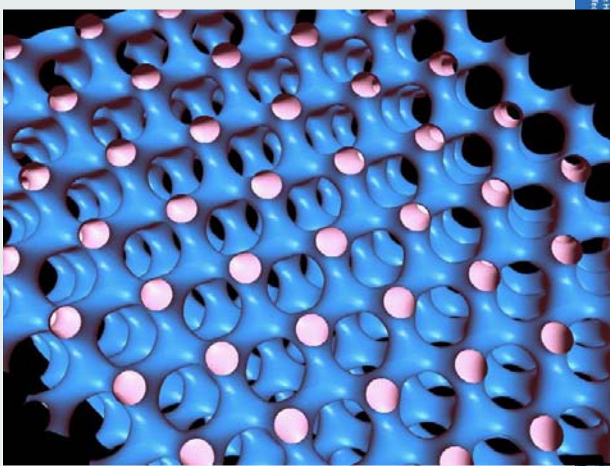

Design of Complex Forms

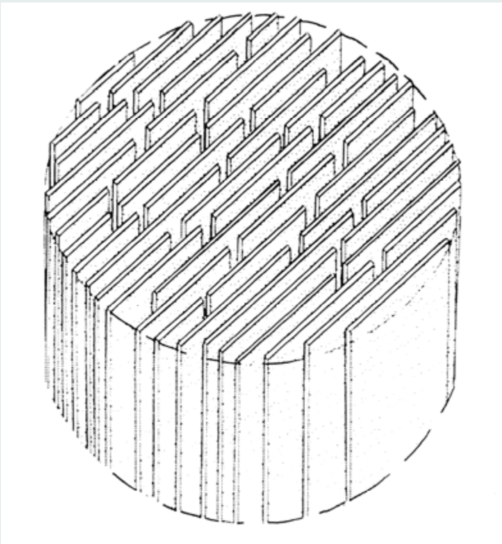

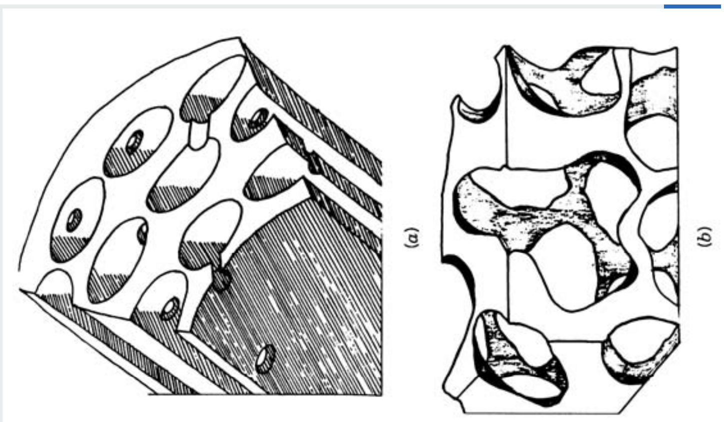

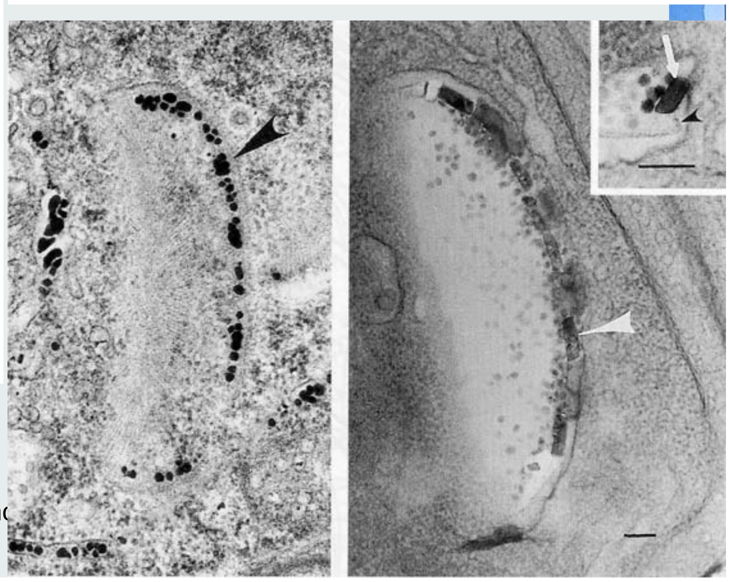

How is it achieved ?

Table 3.2 The main types of biomineralization processes

Process	Control mechanism	Concepts	Properties	Chapter
Precipitation (crystallization)	Chemical	Solubility Supersaturation Nucleation Growth	Solution composition Promotion Inhibition Phase transformation	4
Boundary-organized biomineralization	Spatial	Supramolecular preorganization	Physical boundary Diffusion-limited site Ion transport Size and shape Organization	5
Organic matrix-mediated biomineralization	Structural	Interfacial molecular recognition	Site-directed nucleation Oriented nucleation Supporting framework Mechanical design	6
Morphogenesis	Morphological	Vectorial regulation	Complex form Time-dependent form Patterning	7
Biomineral tectonics	Constructional	Multilevel processing	Higher-order assembly Hierarchical structures Integrative building modules Adaptive structures and functions	8

What is achieved ?

- uniform particle sizes
- well-defined structures and compositions
- high levels of spatial organization
- complex morphologies
- controlled aggregation and texture
- preferential crystallographic orientation
- higher-order assembly into hierarchical structures.

What is achieved ?

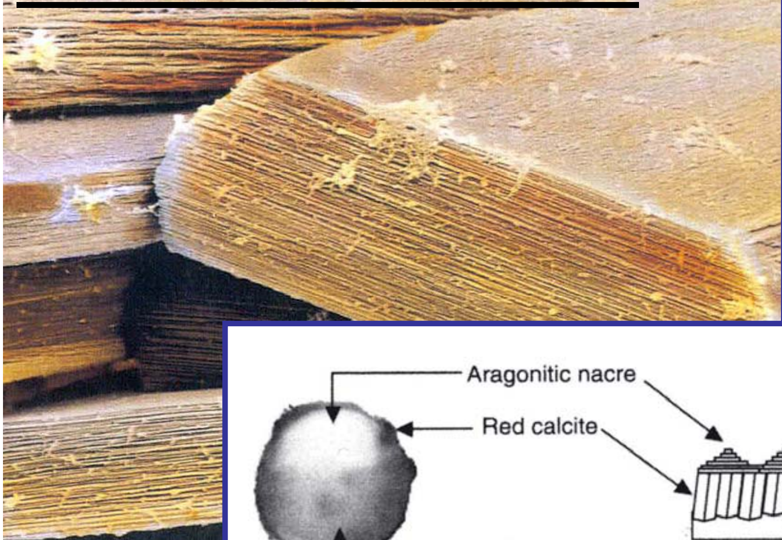

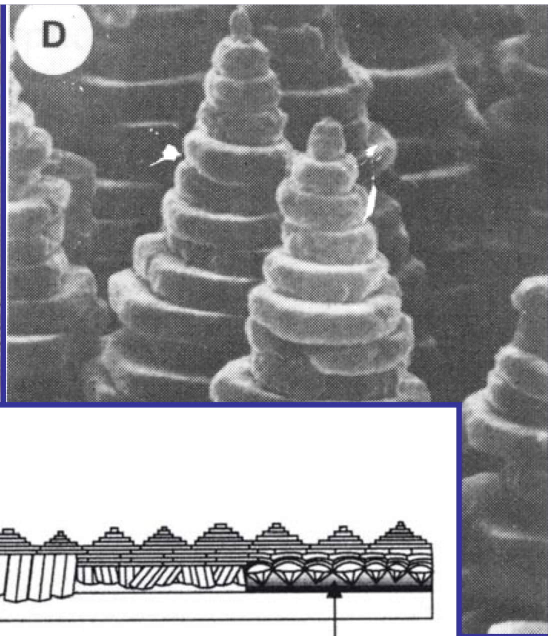

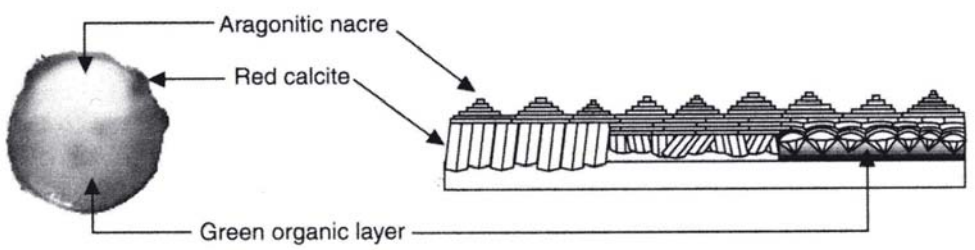

Figure 15.3 A mature flat pearl. The c-axis of the nacre is perpendicular to the paper. The three different regions of the flat pearl are labeled red calcite, aragonitic nacre and green organic layer. The schematic diagram on the right shows the spatial organization of the regions.

Toughness

Structural basis for the fracture toughness of the shell of the conch *Strombus gigas*

S. Kamat*, X. Su*, R. Ballarini† & A. H. Heuer*

Nature 405 (2000) 1038

Layers : 0.5-2mm
1. Order lamella : 5-60mm
2. Order lamella : 5-30mm
3. Order lamella : 60-130nm

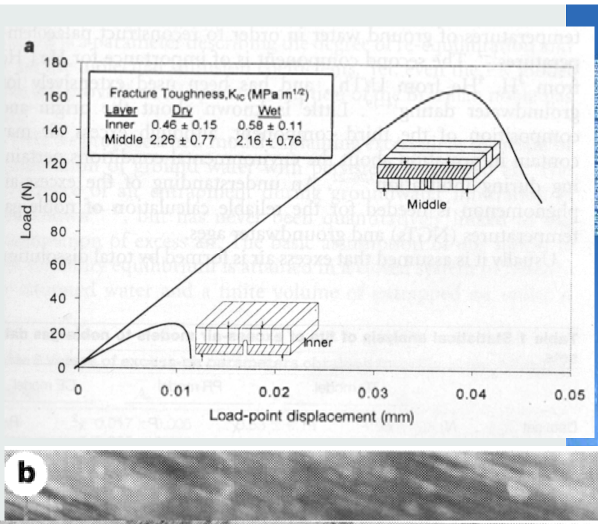

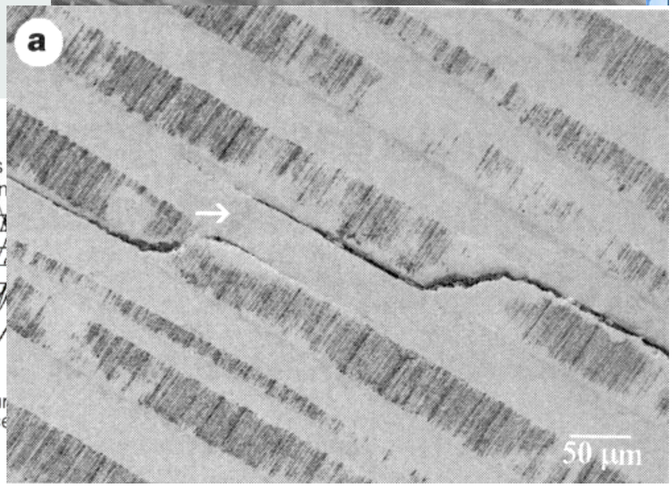

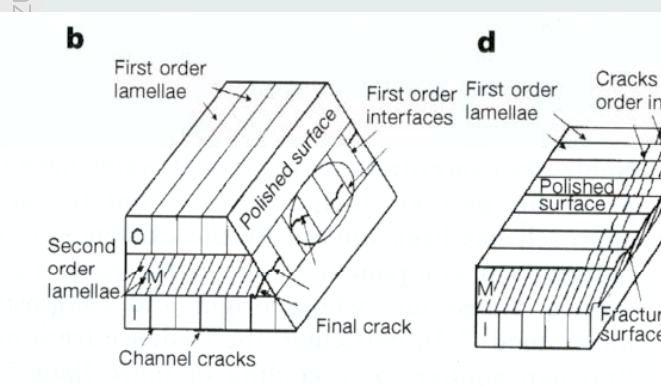

Design of Complex Forms - Diatoms

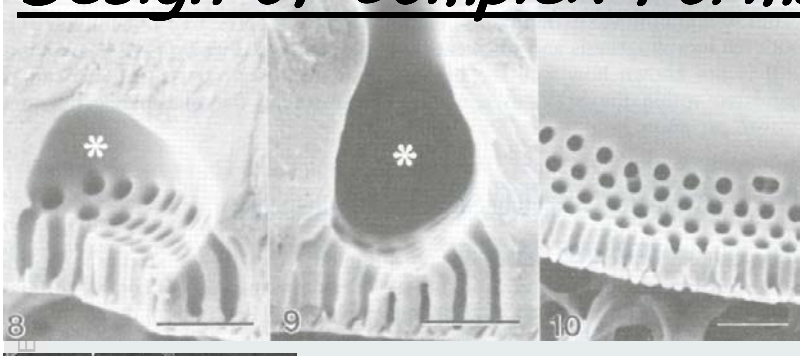

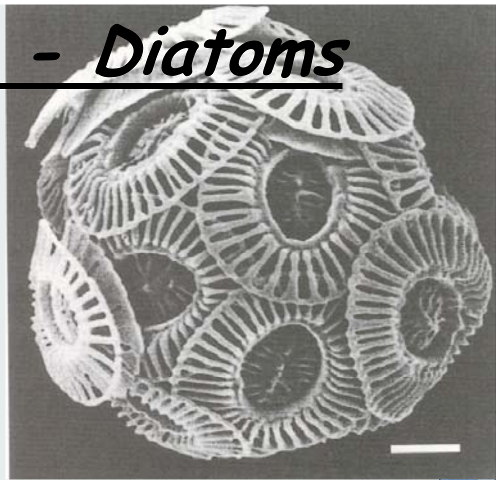

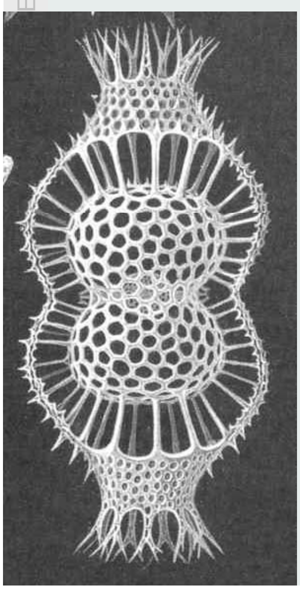

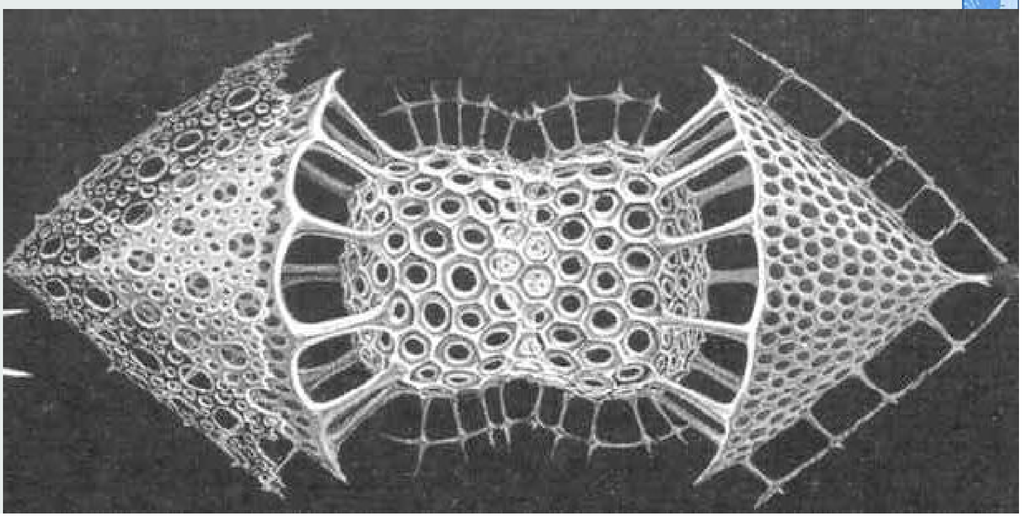

How is it achieved ?

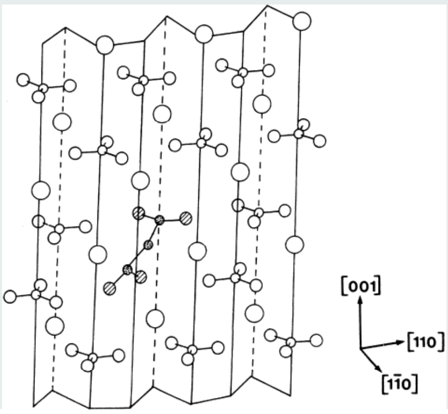

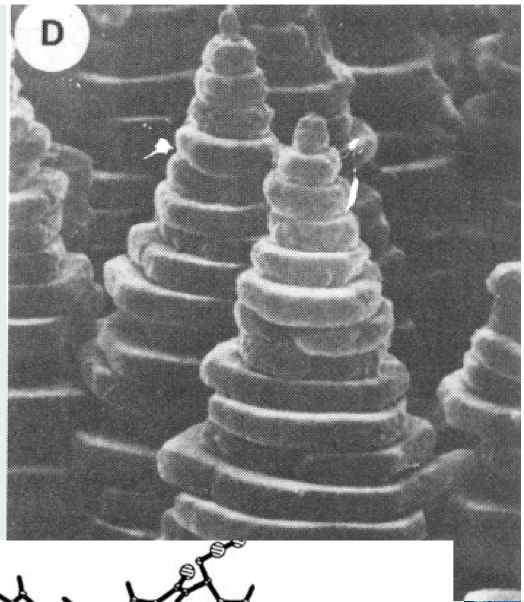

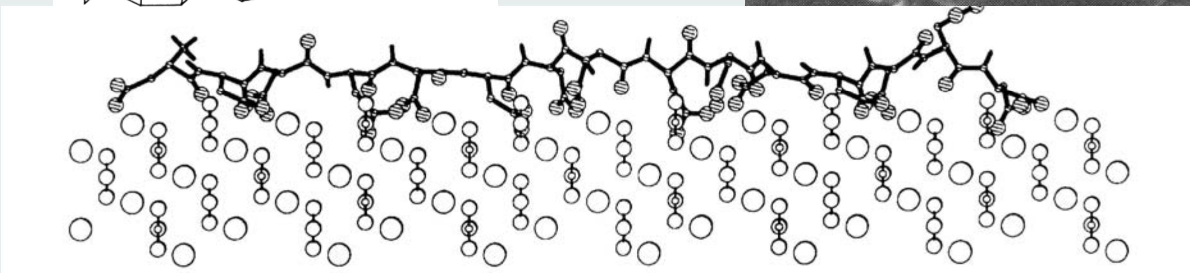

Fig. 4.23 Computer model showing side view of the calcite {1$\bar{1}$0} face with surface-bound polyaspartate ($[Asp]_{11}$).

Control and Function

- chemical
- spatial
- structural
- morphological
- constructional.

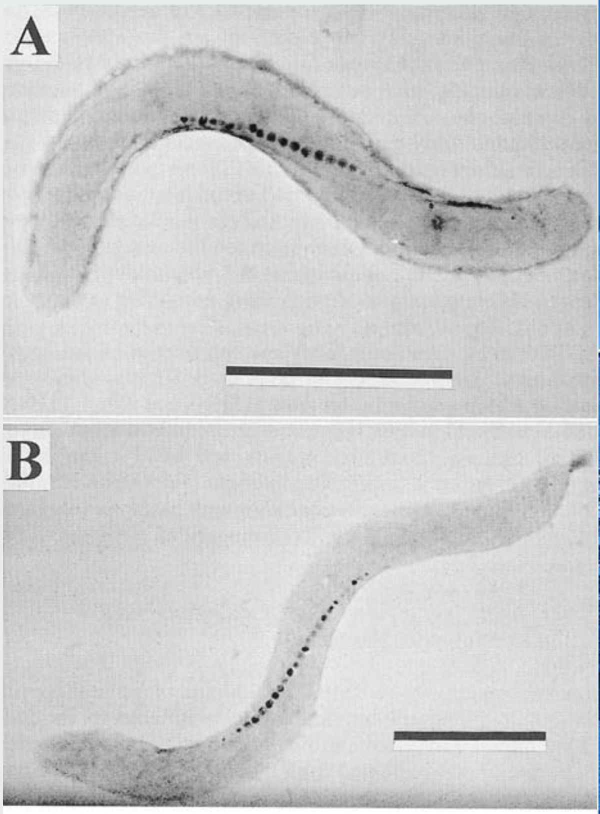

Control and Function

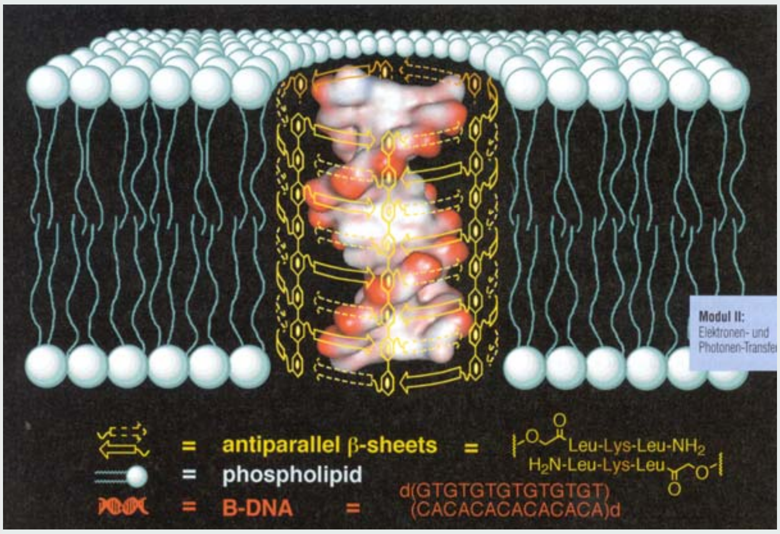

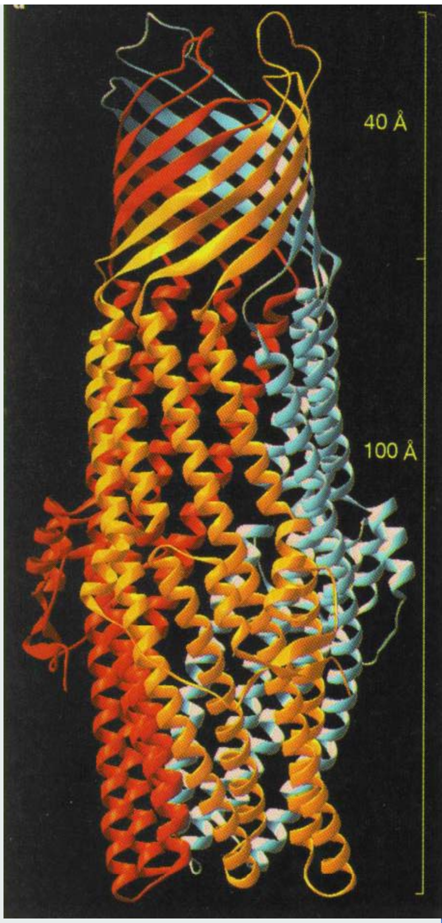

Structural Alignment

organic matrix / mould

Composite organic + α–FeOOH

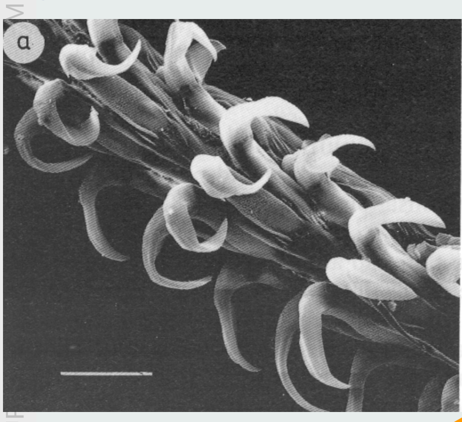

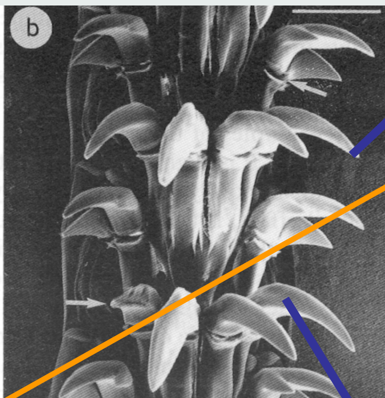

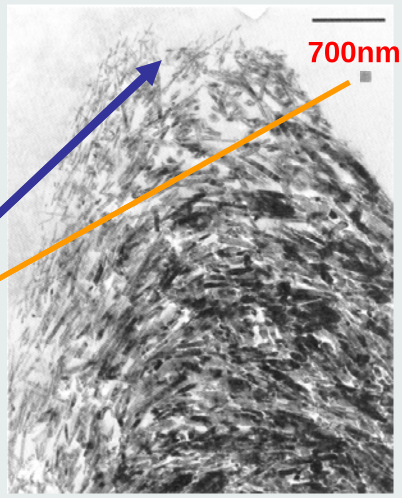

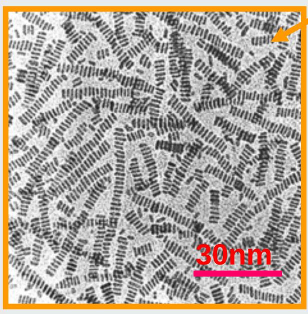

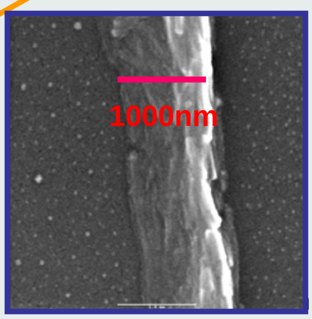

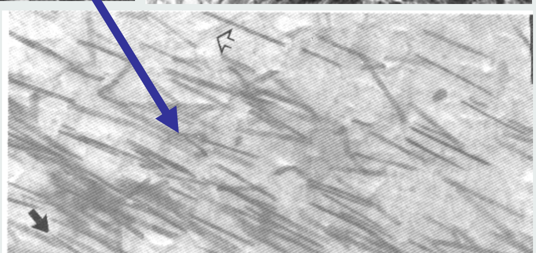

J.Webb, D.J. Macey, S. Mann
in S. Mann, J.Webb, R.J.P.Williams,
Biomineralization, VCH 1989

Biodynamic Restoration

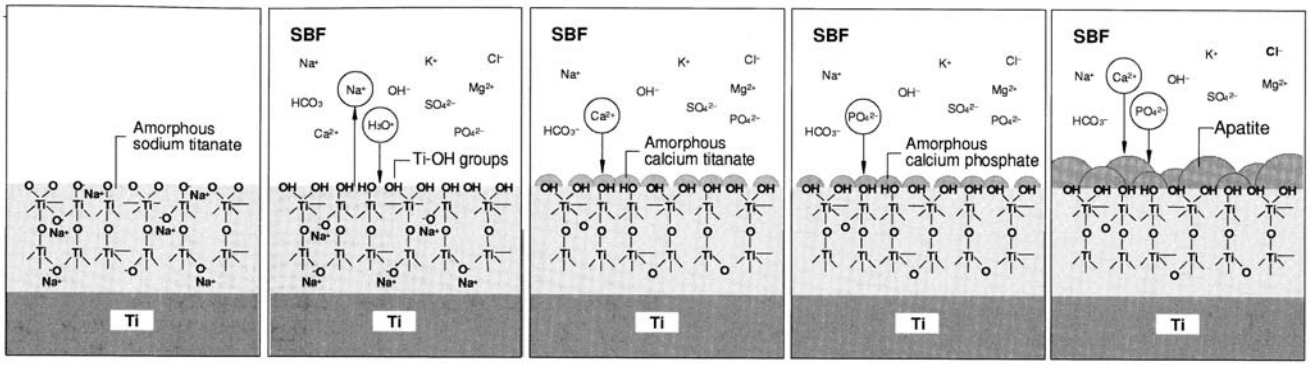

Figure 2. Schematic representation of the mechanism of apatite formation on NaOH-treated Ti metal in simulated body fluid (SBF) (from Reference 10).

Enamel Formation

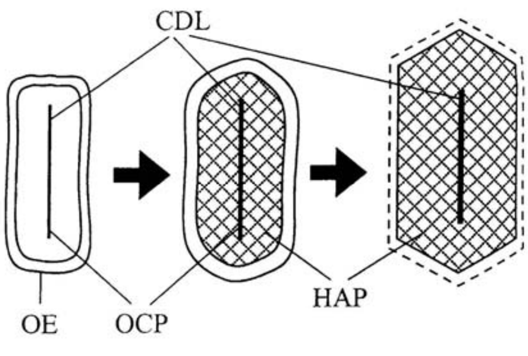

Fig. 4.30 Formation of enamel crystals. An octacalcium phosphate (OCP) precursor phase is formed within an organic envelope (OE) and then overgrown with a single crystal of hydroxyapatite (HAP). Traces of the OCP phase are left as a central dark line (CDL) inside the mature crystal.

Table 4.2 Epitaxial deposition of inorganic crystals on inorganic substrates. A positive percentage misfit value indicates that the overgrowth lattice is larger than the substrate lattice

Substrate	Overgrowth	Lattice misfit %
PbS	NaI	8
	KCl	5
	NaBr	−1
	NaCl	−6
	AgBr	−4
	AgCl	−7
$CaCO_3$	RbBr	7
	RbCl	3
	KBr	3
	NaI	1
	KCl	−2
	NaBr	−7
CaF_2	NaBr	8
	NaCl	3
	LiBr	0
	LiCl	−6
NaCl	NaBr	6
	NaCN	6
	AgBr	3
	AgCN	3
	AgCl	1
	KF	−5

Living System

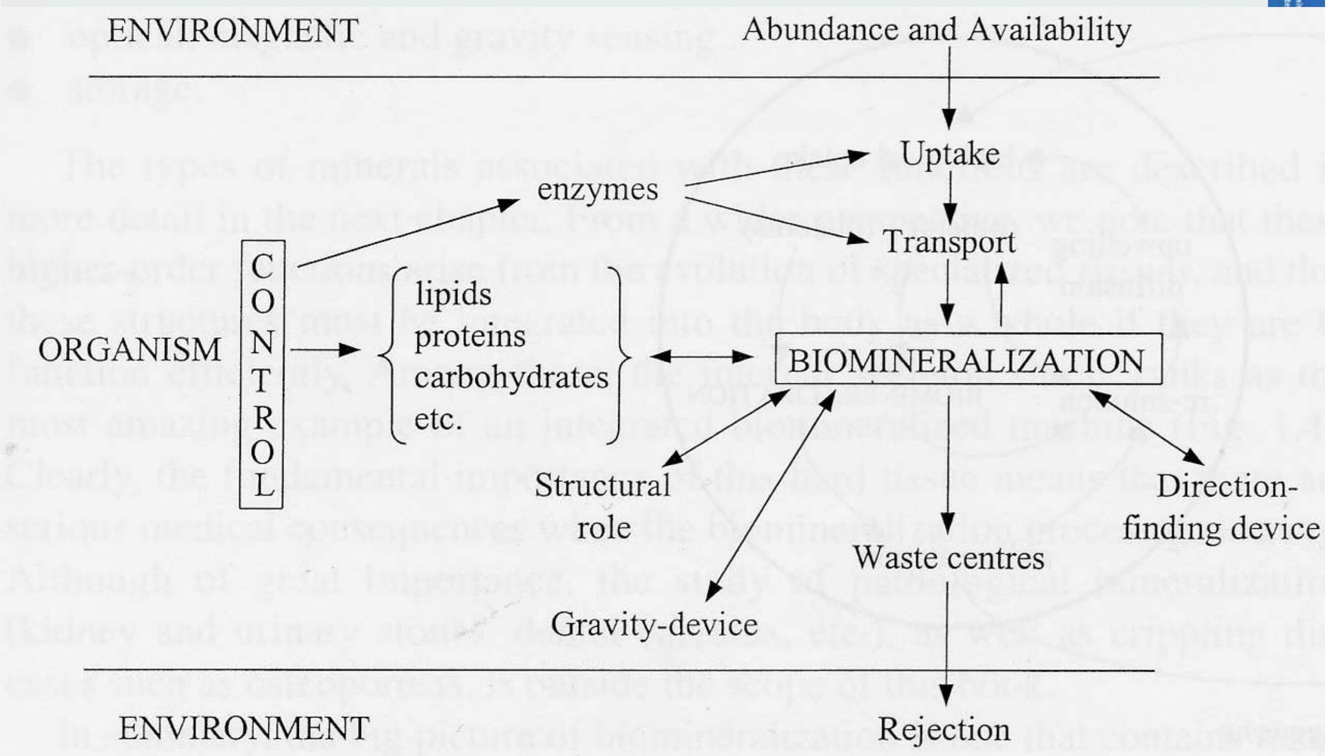

Living System

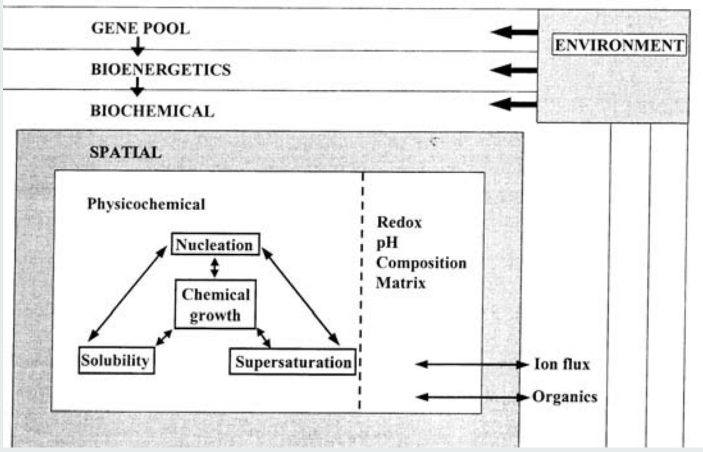

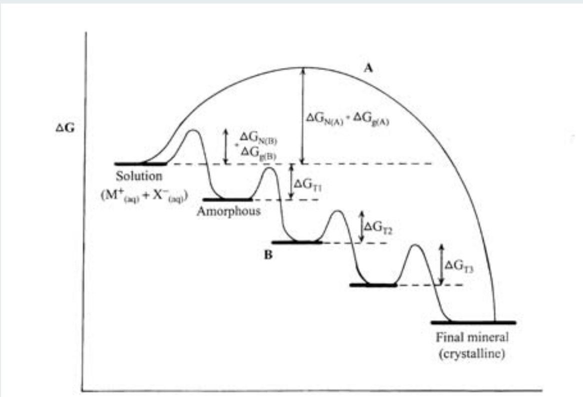

Fig. 4.25 Pathways to crystallization and polymorph selectivity: (A) direc (B) sequential. See text for details.

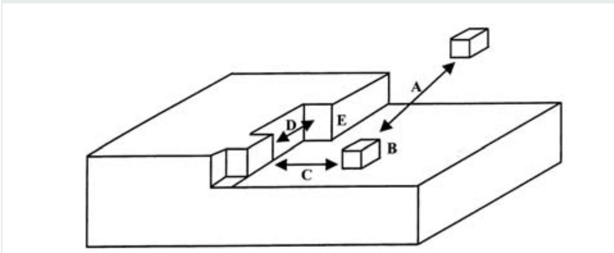

Fig. 4.6 Layer-by-layer mechanism of crystal growth. See text for details.

Biosensors

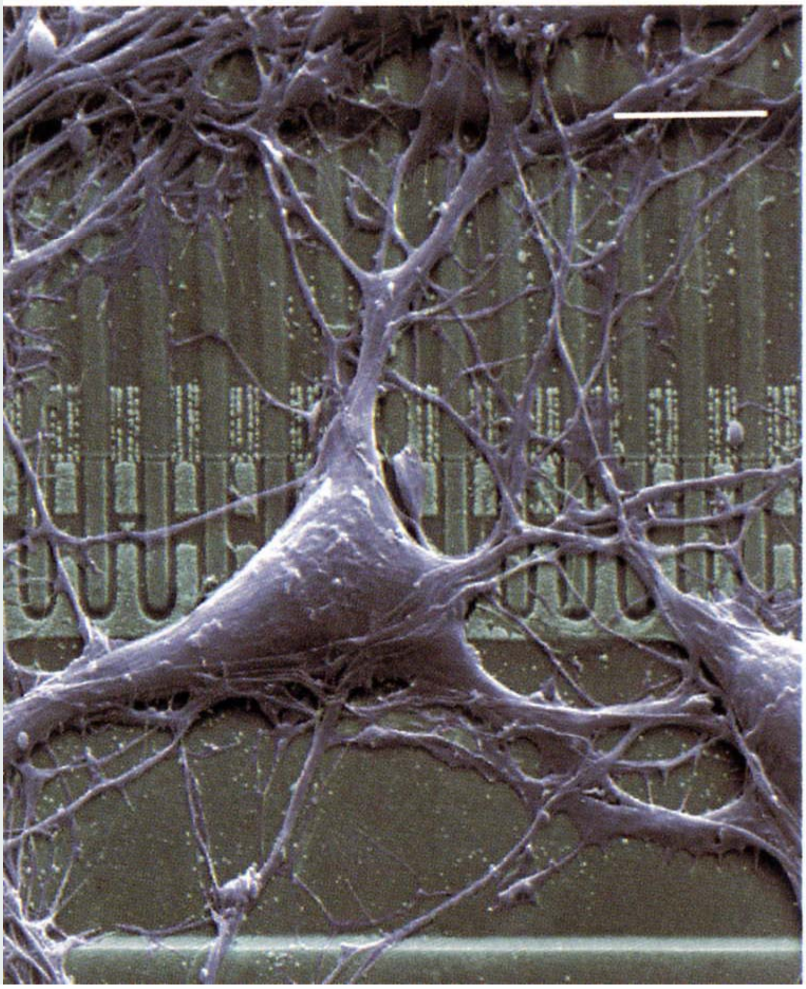

Tumor + Gene Therapy

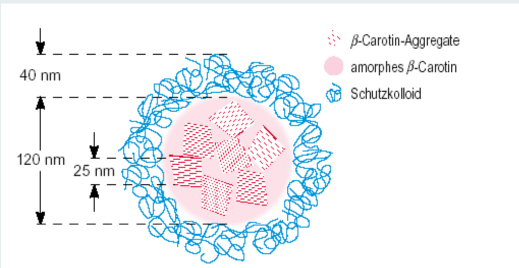

Abbildung 27. Kern-Schale-Aufbau der β-Carotin-Hydrosol-Partikel. Den spektroskopischen Daten und den Weitwinkelröntgenspektren (WAXS) zufolge besteht der Wirkstoff-Kern aus H- und J-Aggregaten mit Abmessungen bis zu 30 nm, entsprechend einer maximalen Aggregationszahl von 10000 Molekülen.